Electronic Supplementary Material (ESI) for Chemical Science.

***Supporting Information for:***

# Structure and Bonding in Rhodium Coordination Compounds: A $^{103}$Rh Solid-State NMR and Relativistic DFT Study

Sean T. Holmes,[1,2] Jasmin Schönzart,[1,2] Adam B. Philips,[3] James J. Kimball,[1,2]
Sara Termos,[1,2] Adam R. Altenhof,[1,2] Yijue Xu,[2] Christopher A. O'Keefe,[4]
Jochen Autschbach,[3,*] Robert W. Schurko[1,2*]

[1] Department of Chemistry & Biochemistry, Florida State University, Tallahassee, FL 32306
[2] National High Magnetic Field Laboratory, Tallahassee, FL 32310
[3] Department of Chemistry, University at Buffalo, State University of New York, Buffalo, NY 14260-3000
[4] Department of Chemistry & Biochemistry, University of Windsor, Windsor, ON, Canada N9B 3P4

* Authors to whom correspondence should be addressed
E-mail: rschurko@fsu.edu, jochena@buffalo.edu

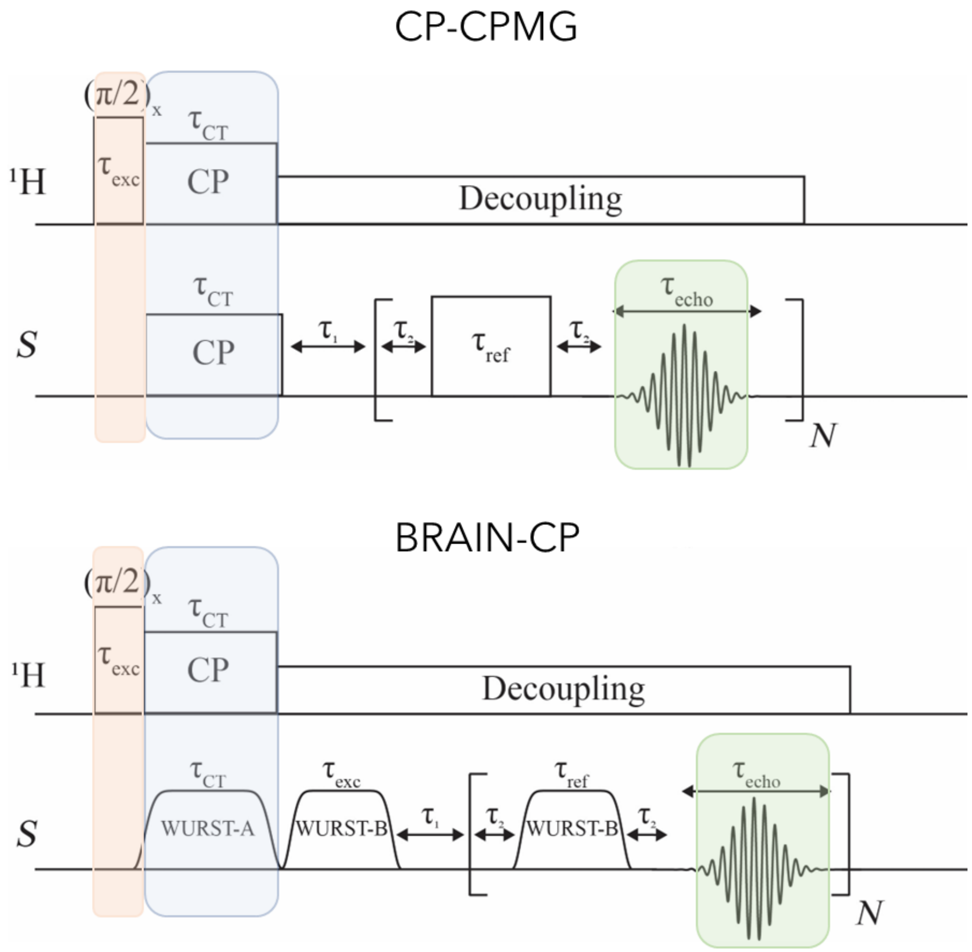

**Scheme S1.** Illustrations of the CP-CPMG and BRAIN-CP pulse sequences.

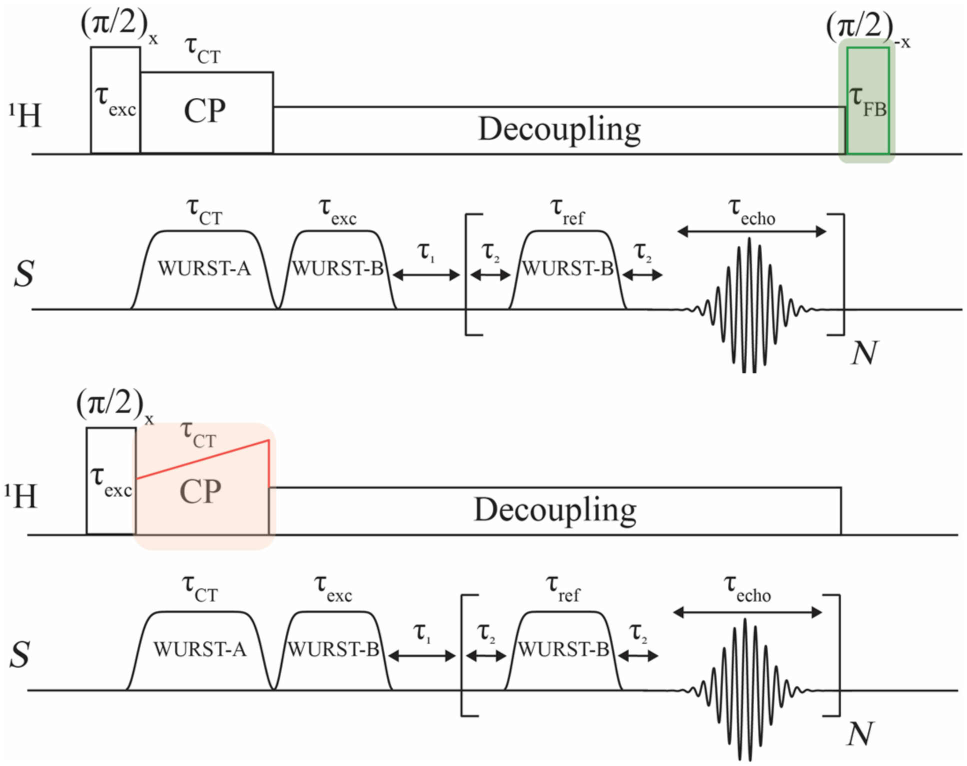

**Scheme S2.** Illustration of the BRAIN-CP pulse sequence, with modifications highlighted: (i) the inclusion of a flip-back pulse (green box) can potentially reduce the recycle delay; (ii) a ramped-amplitude $^{1}$H spin-lock pulse (orange box) compensates for rf inhomogeneities at offsets far from the transmitter.

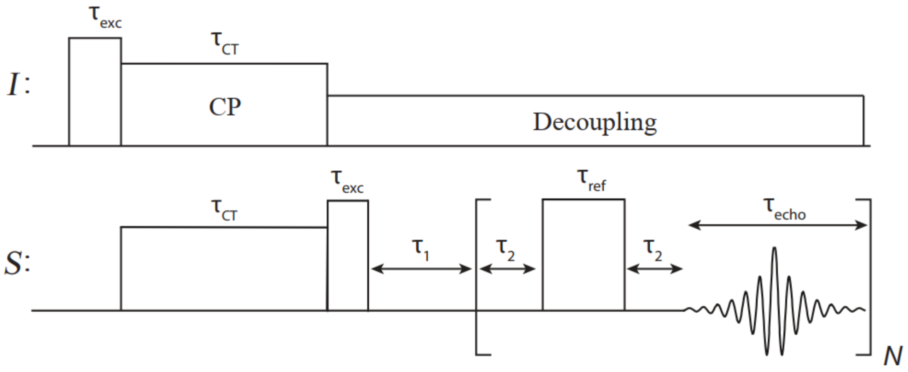

**Scheme S3.** Illustration of the modified CP-CPMG pulse sequence used for rf calibration.

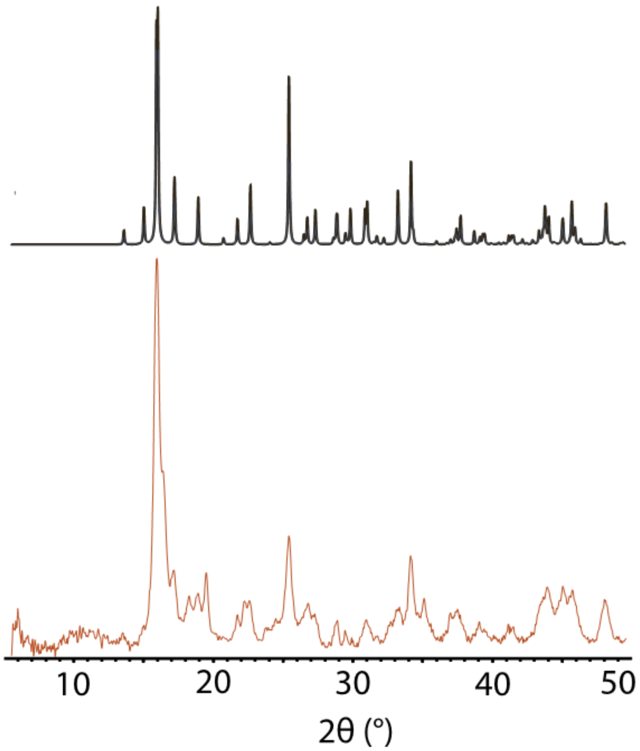

**Figure S1.** Experimental PXRD pattern of $[Rh(NH_3)_5Cl]Cl_2$ in orange, and corresponding simulation based on the known crystal structure (both at 298 K) in black.

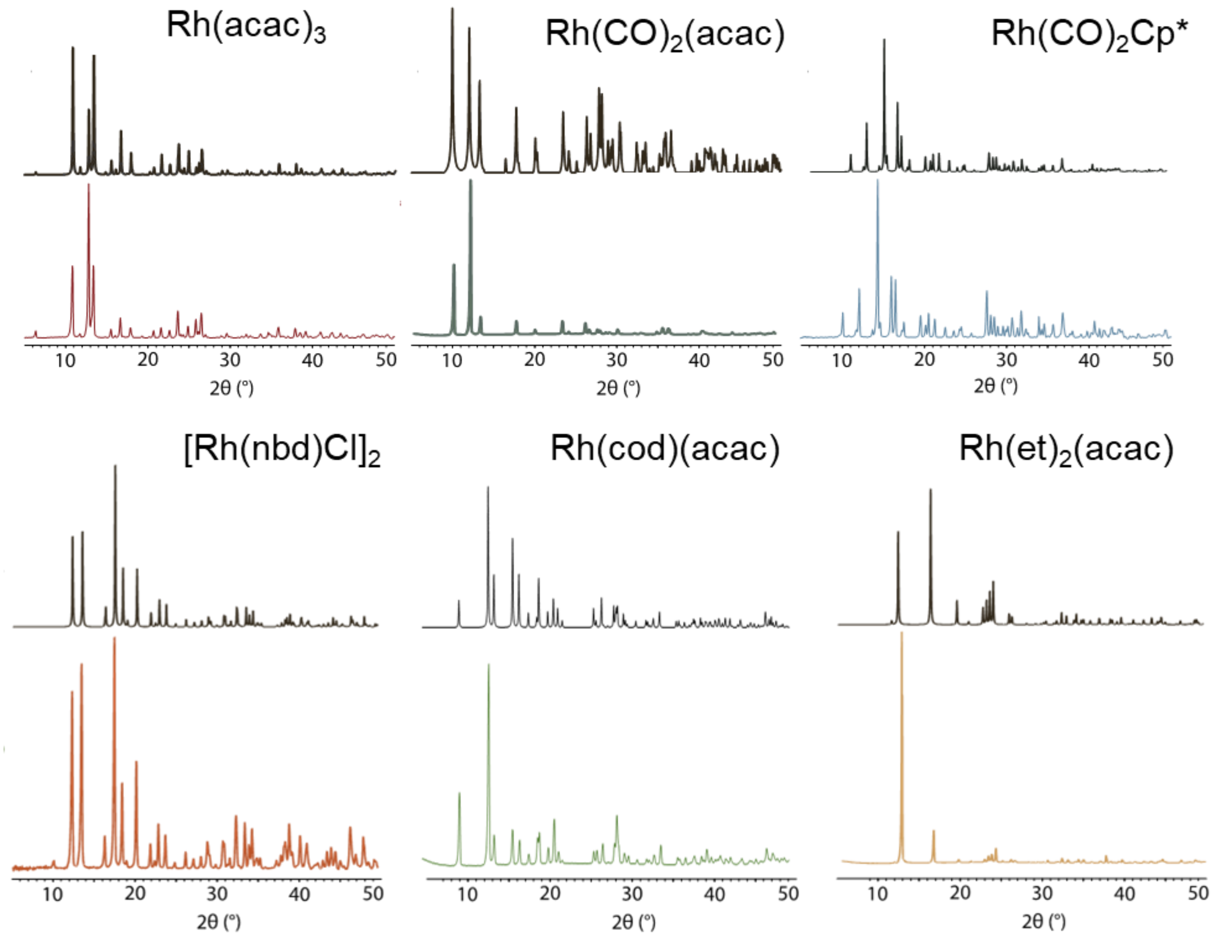

**Figure S2.** Experimental PXRD patterns (colored lines), and corresponding simulations based on the known crystal structures (black lines). An impurity is marked by as asterisk.

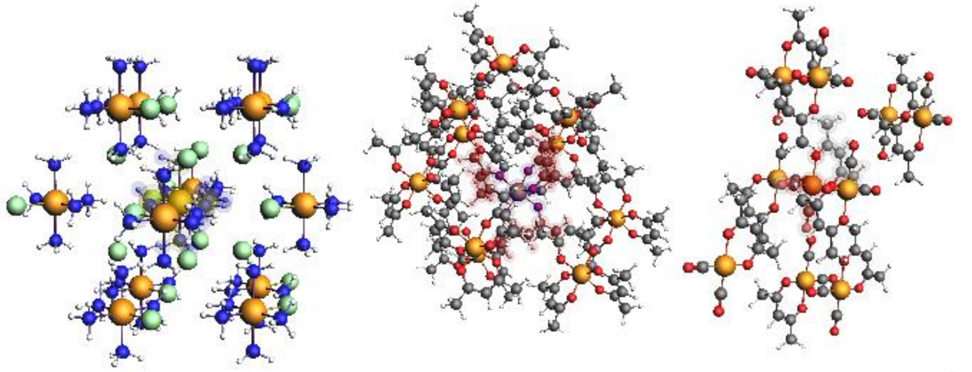

$[RhCl(NH_3)_5]Cl_2$ $Rh(acac)_3$ $Rh(CO)_2(acac)$

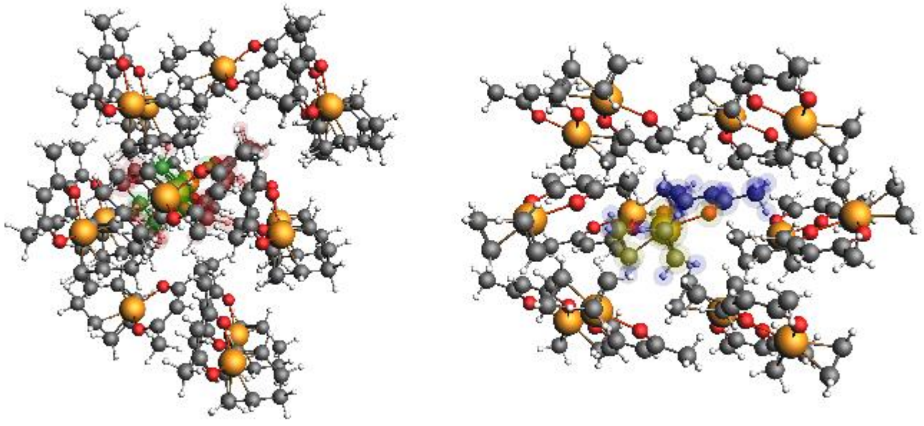

Rh(cod)(acac) $Rh(et)_2(acac)$

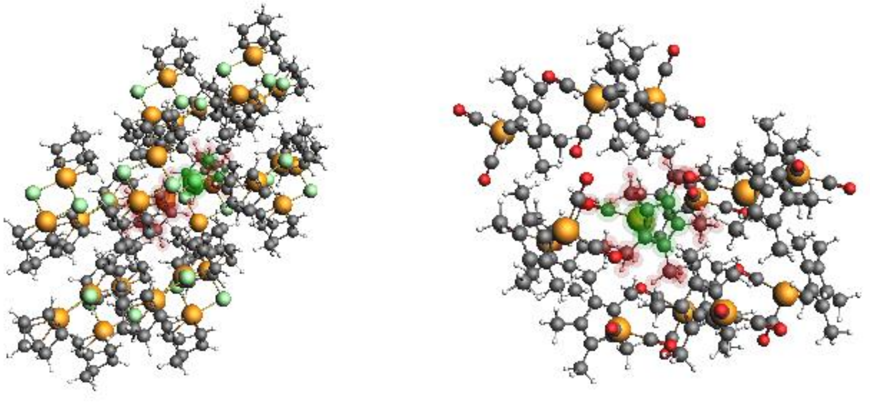

$[Rh(nbd)Cl]_2$ $Rh(CO)_2Cp^*$

**Figure S3.** Clusters models used to model the lattice effects on computed $^{103}$Rh magnetic shielding tensors.

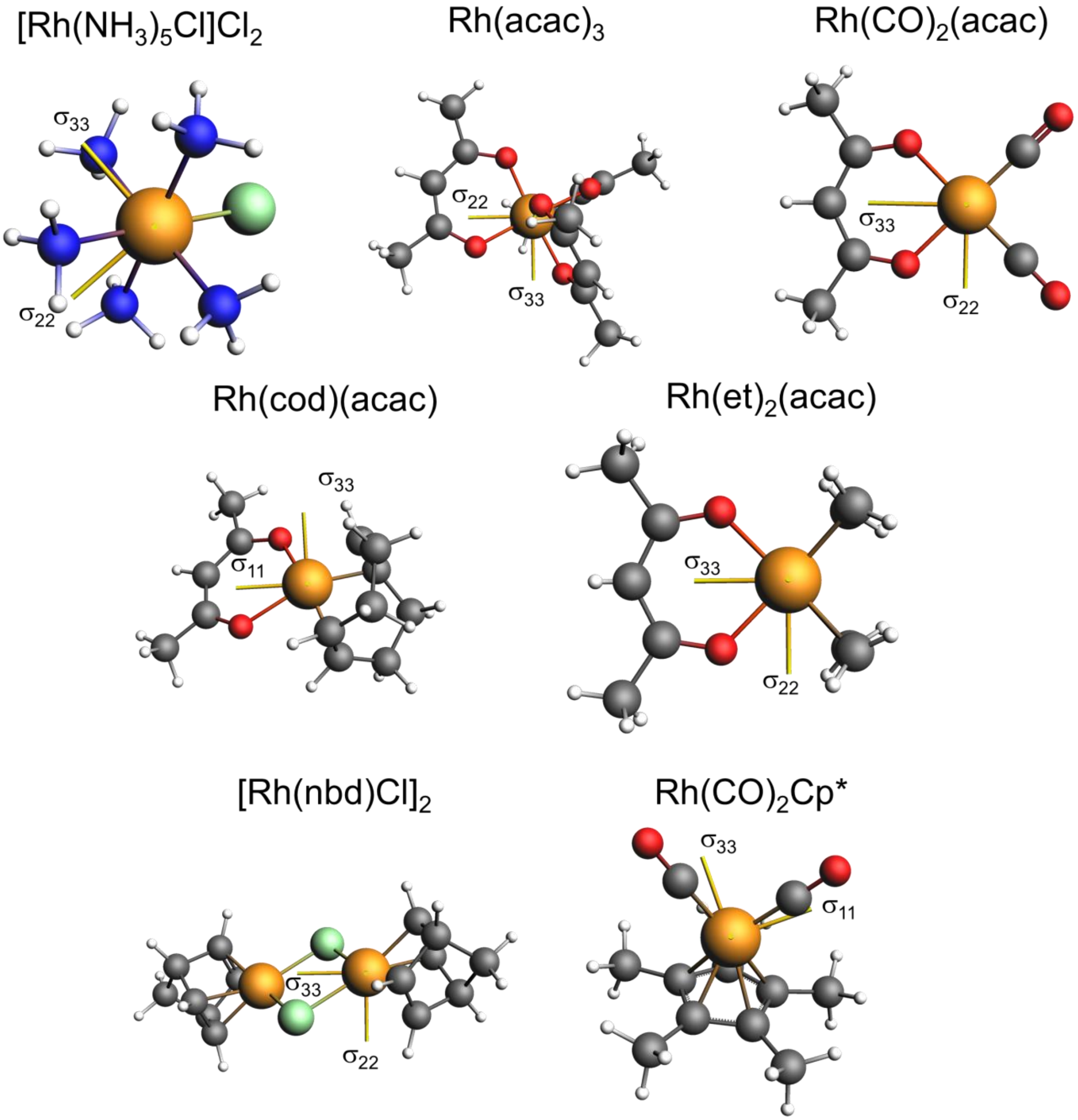

$[Rh(NH_3)_5Cl]Cl_2$

$Rh(acac)_3$

$Rh(CO)_2(acac)$

Rh(cod)(acac)

$Rh(et)_2(acac)$

$[Rh(nbd)Cl]_2$

$Rh(CO)_2Cp^*$

**Figure S4.** Orientations of the principal values of the $^{103}$Rh magnetic shielding tensors, as calculated at the PBE0/SO level. The yellow vectors show the orientations of two principal values, with the third oriented perpendicular to the page.

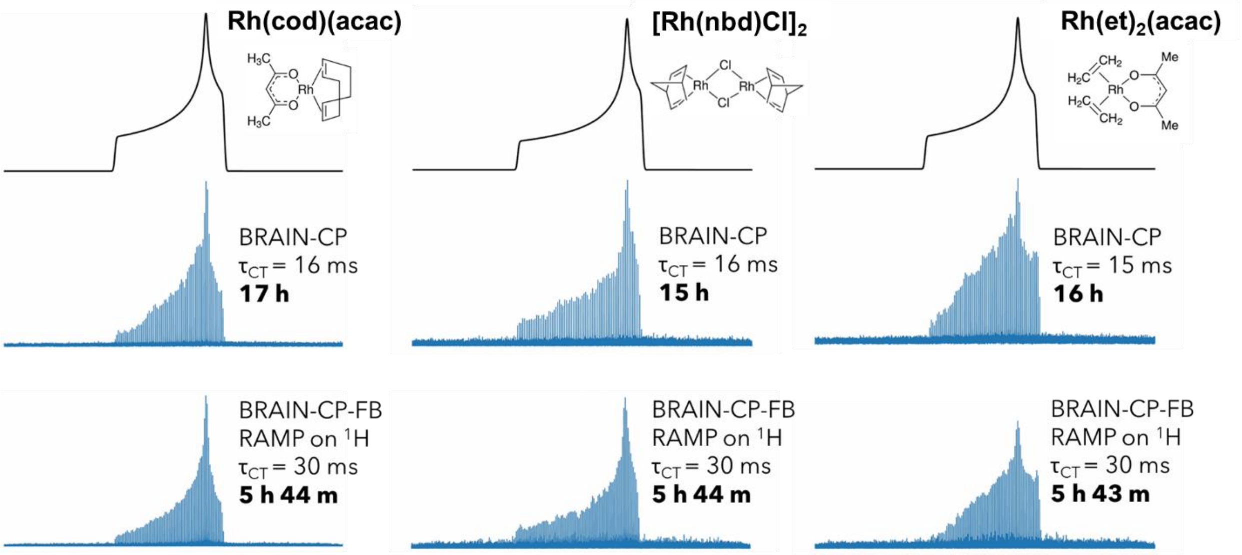

**Figure S5.** The combination of long contact pulses of 30 ms, ramped-amplitude $^1$H spin-lock pulses, and flip-back pulses greatly reduces experimental times, relative to experiments acquired using shorter contact pulses (15 – 16 ms), constant-amplitude $^1$H spin-lock pulses, and no flip-back pulse. All data were acquired at 21.1 T using the BRAIN-CP sequence.

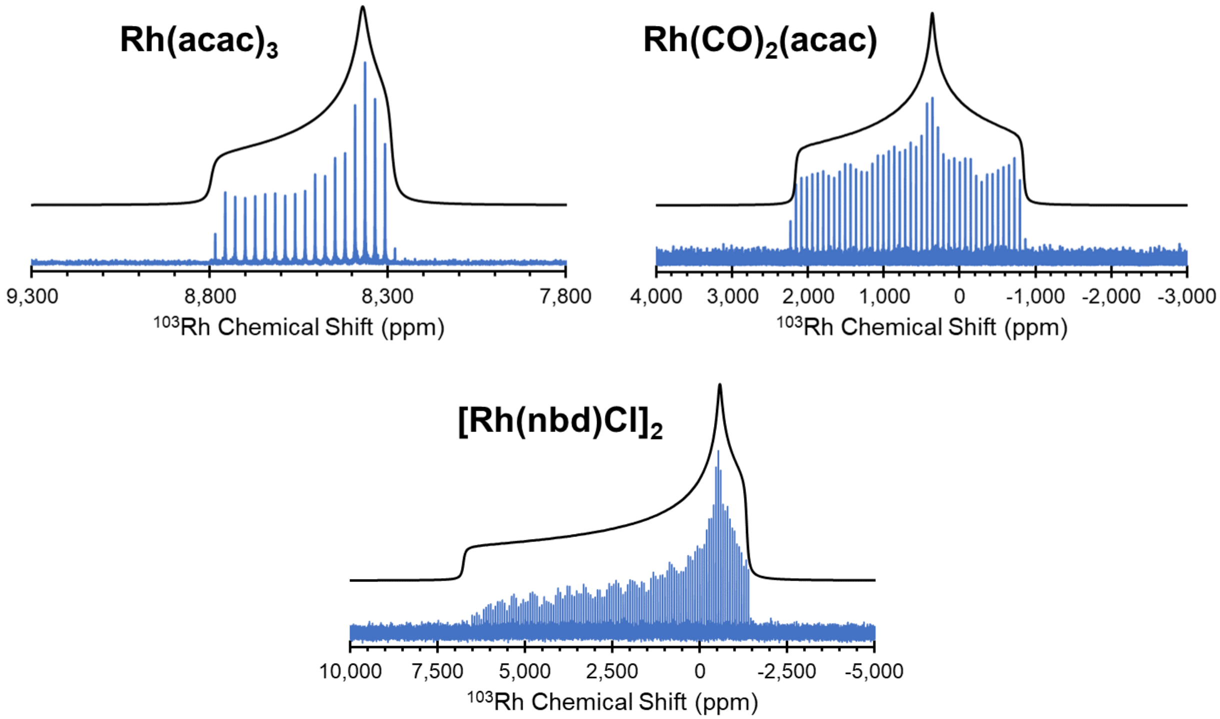

**Figure S6.** $^1$H-$^{103}$Rh BRAIN-CP spectra acquired at 35.2 T for Rh(acac)$_3$, Rh(CO)$_2$(acac), and [Rh(nbd)Cl]$_2$.

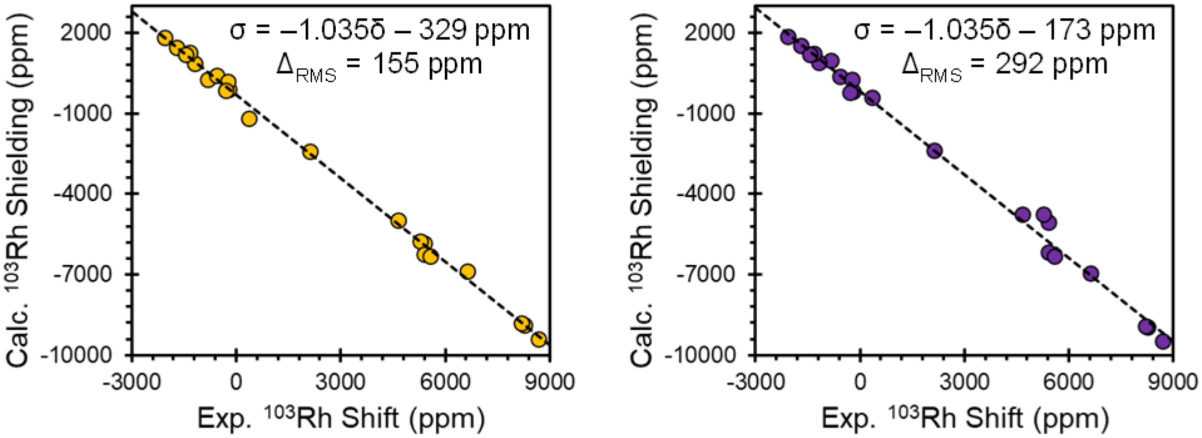

**Figure S7.** Calculations of $^{103}$Rh magnetic shielding tensors using complete first coordination shell clusters of molecules (yellow) or isolated molecules (purple) as structural models. All calculations were performed at the PBE0/SO level. Black lines represent the best fits, with the equations provided.

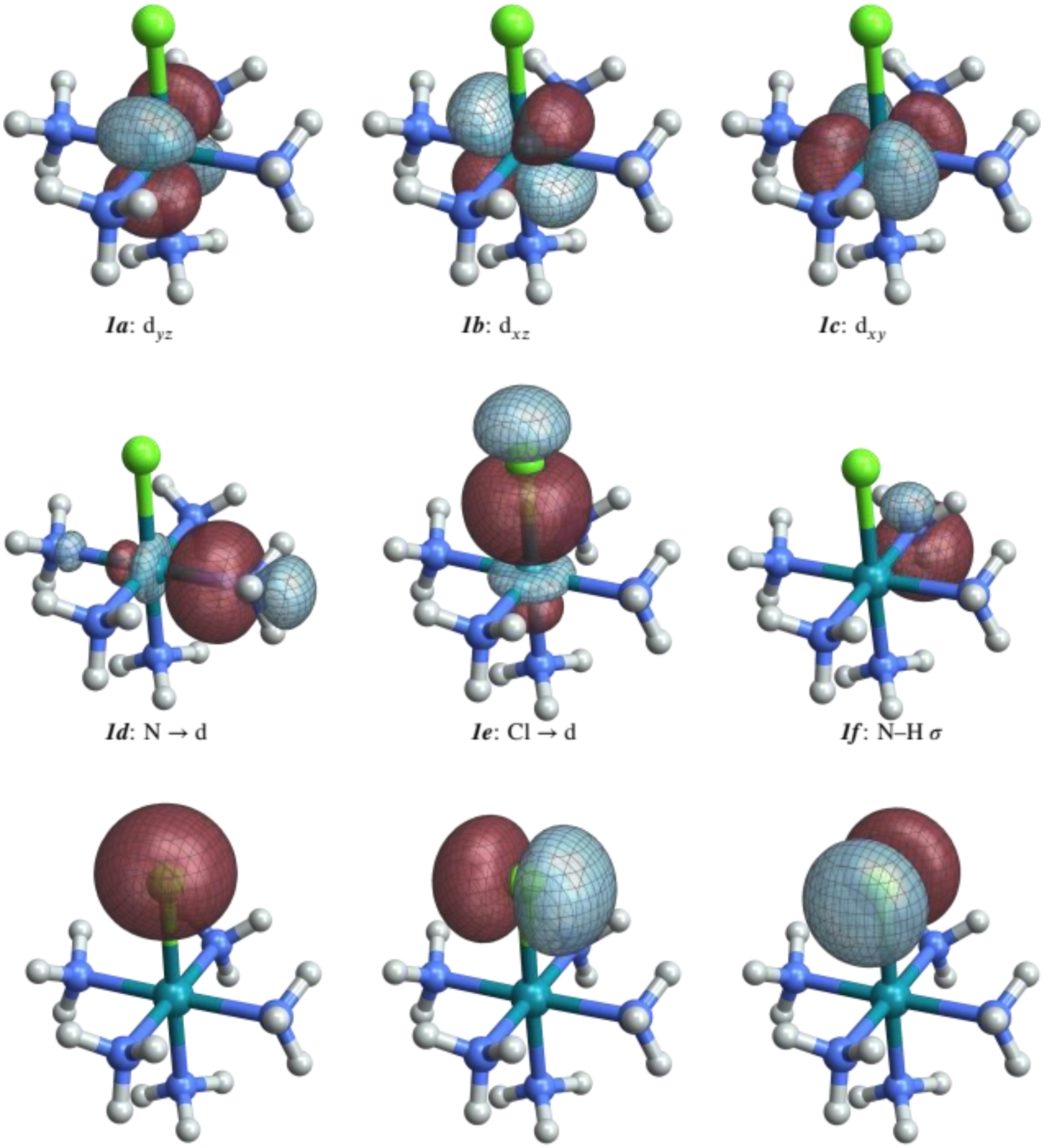

***Ia***: $d_{yz}$ ***Ib***: $d_{xz}$ ***Ic***: $d_{xy}$

***Id***: N → d ***Ie***: Cl → d ***If***: N–H $\sigma$

***Ig***: Cl s ***Ih***: Cl $p_x$ ***Ii***: Cl $p_y$

**Figure S8.** Isosurfaces for primary NLMO contributions to Rh isotropic shielding in $[Rh(NH_3)_5Cl]^{2+}$.

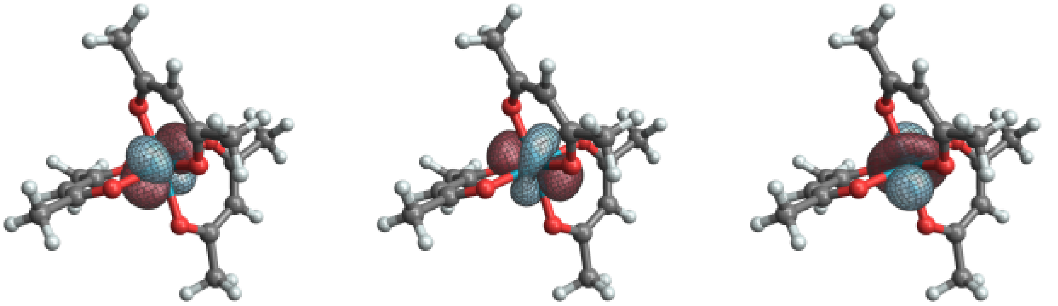

***2a***: $d_{nb}$ ***2b***: $d_{nb}$ ***2c***: $d_{nb}$

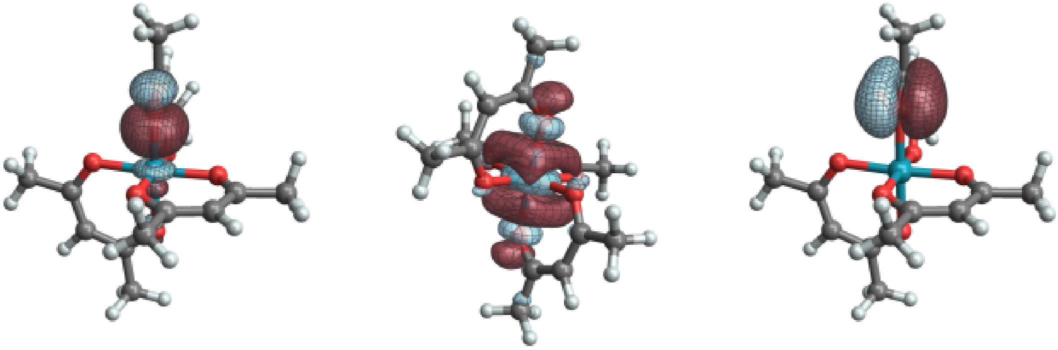

***2d***: acac O → d ***2e***: 5s-like $\sigma^*$ ***2f***: acac C–O $\pi$

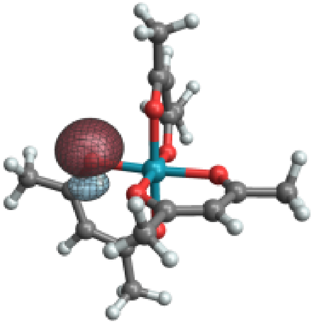

***2g***: acac O LP

**Figure S9.** Isosurfaces for primary NLMOs contributing to the Rh isotropic shielding in Rh(acac)$_3$.

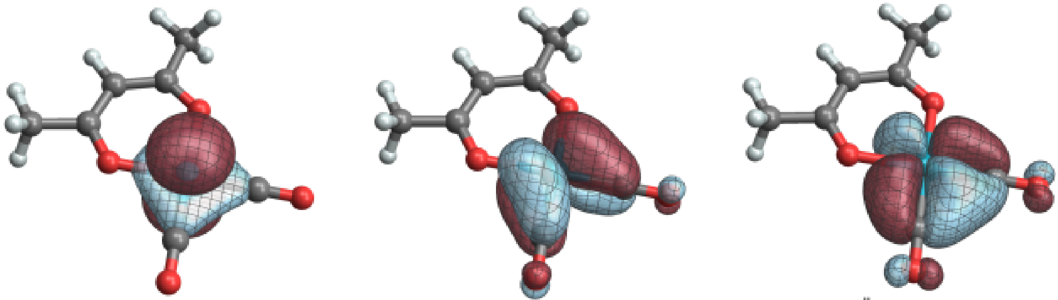

***3a***: $d_{z^2} \rightarrow \mathrm{CO}$ ***3b***: $d_{\pi} \rightarrow \mathrm{CO}$ ***3c***: $d_{\pi}^{\parallel} \rightarrow \mathrm{CO}$

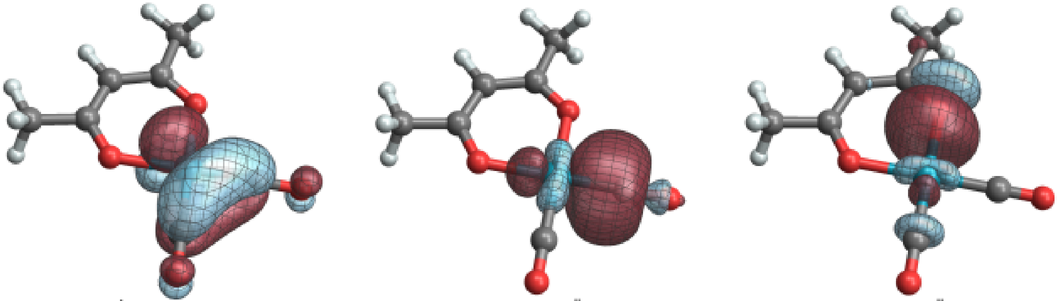

***3d***: $d_{\pi}^{\perp} \rightarrow \mathrm{CO}$ ***3e***: $\mathrm{CO} \rightarrow d^{\parallel}$ ***3f***: acac $\rightarrow d^{\parallel}$

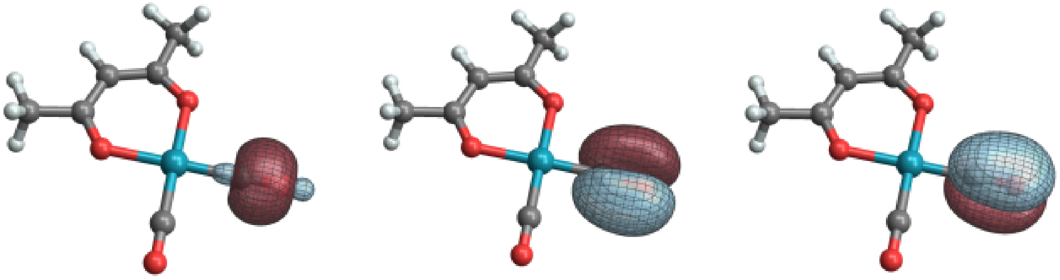

***3g***: CO $\sigma$ ***3h***: CO $\pi_1$ ***3i***: CO $\pi_2$

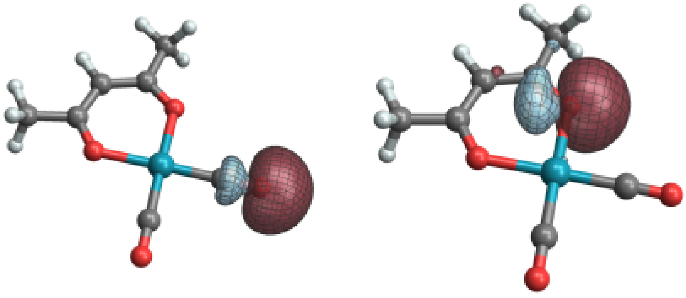

***3j***: CO O LP ***3k***: acac O LP

**Figure S10.** Isosurfaces for primary NLMOs contributing to the Rh isotropic shielding in Rh(CO)$_2$(acac).

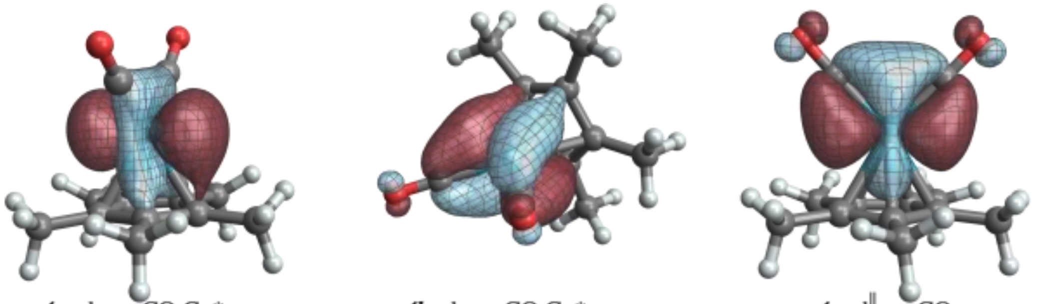

***4a***: $d_{\delta} \rightarrow$ CO,Cp* ***4b***: $d_{\delta} \rightarrow$ CO,Cp* ***4c***: $d_{\pi}^{\parallel} \rightarrow$ CO

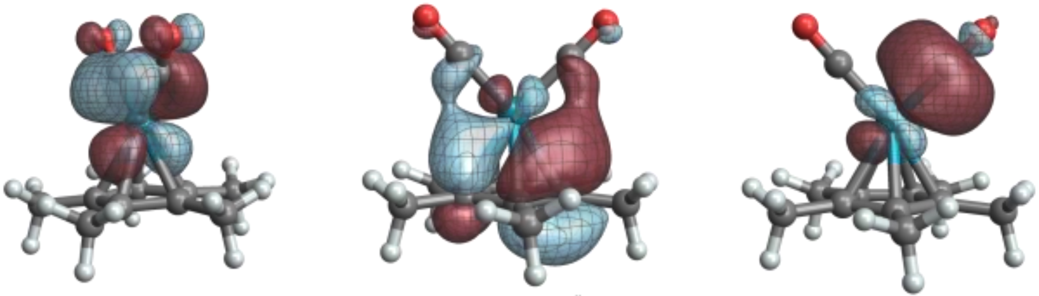

***4d***: $d_{\pi}^{\perp} \rightarrow$ CO ***4e***: Cp* $\rightarrow d_{\pi}^{\parallel}$ ***4f***: CO → d

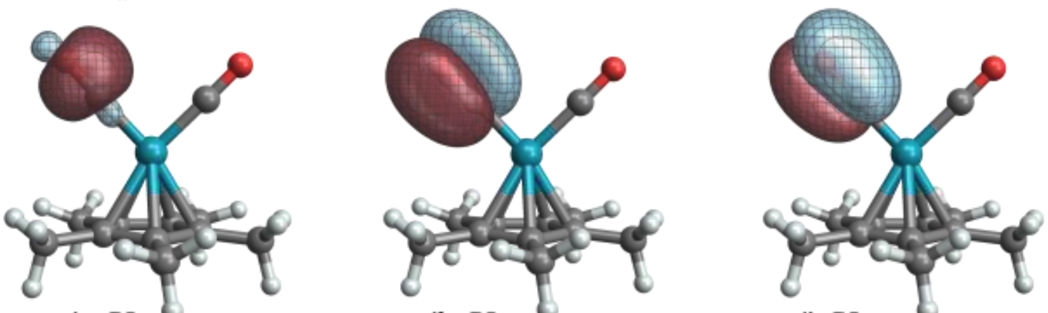

***4g***: CO $\sigma$ ***4h***: CO $\pi_1$ ***4i***: CO $\pi_2$

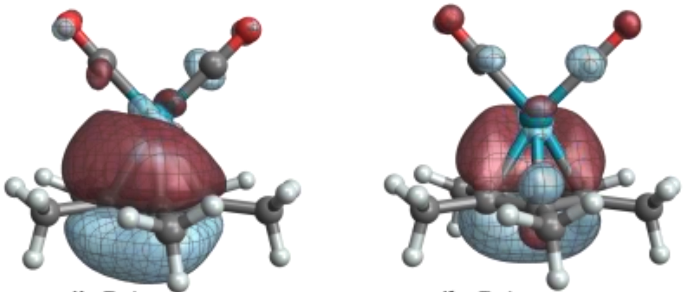

***4j***: Cp* $\pi_1$ ***4k***: Cp* $\pi_2$

**Figure S11.** Isosurfaces for primary NLMOs contributing to the Rh isotropic shielding in $Rh(CO)_2Cp^*$.

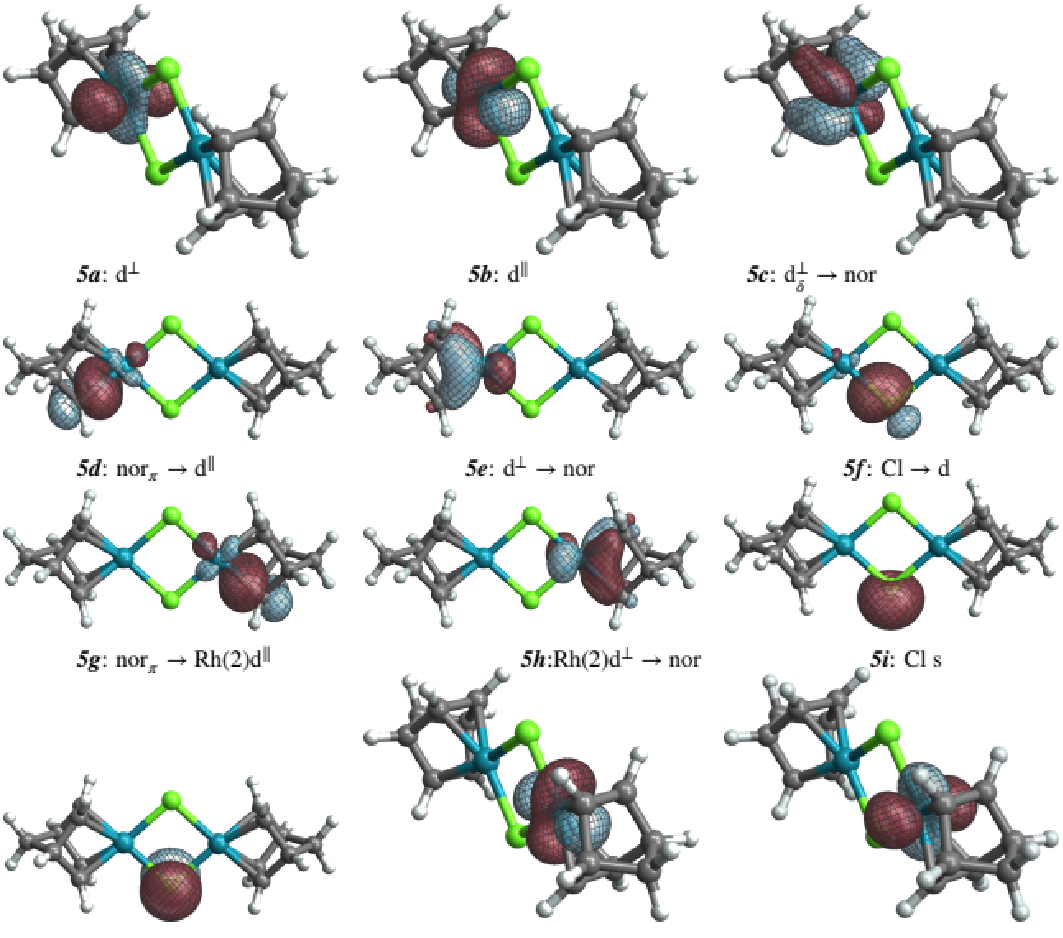

***5a***: $d^{\perp}$

***5b***: $d^{\parallel}$

***5c***: $d_{\delta}^{\perp} \rightarrow \mathrm{nor}$

***5d***: $\mathrm{nor}_{\pi} \rightarrow d^{\parallel}$

***5e***: $d^{\perp} \rightarrow \mathrm{nor}$

***5f***: $\mathrm{Cl} \rightarrow d$

***5g***: $\mathrm{nor}_{\pi} \rightarrow \mathrm{Rh}(2)d^{\parallel}$

***5h***: $\mathrm{Rh}(2)d^{\perp} \rightarrow \mathrm{nor}$

***5i***: Cl s

***5j***: Cl $p_{\perp}$

***5k***: $\mathrm{Rh}(2)d^{\parallel}$

***5l***: $\mathrm{Rh}(2)d^{\perp}$

**Figure S12.** Isosurfaces for primary NLMOs contributing to the Rh isotropic shielding in $[\mathrm{Rh(nbd)Cl}]_2$.

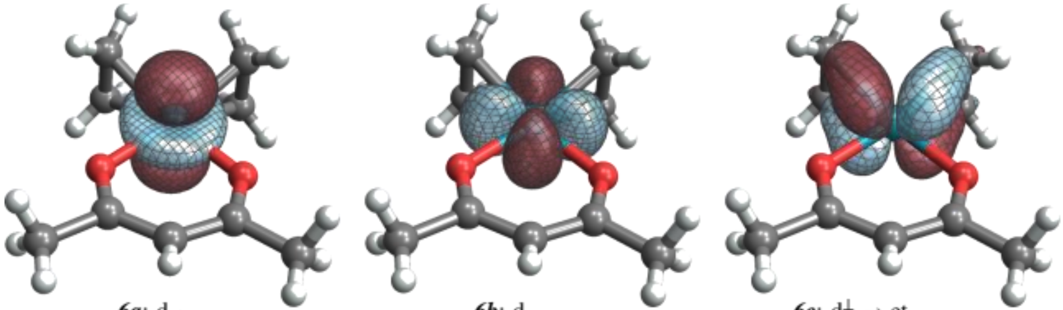

*6a*: $\mathrm{d}_{z^2}$ *6b*: $\mathrm{d}_{xy}$ *6c*: $\mathrm{d}_{\delta}^{\perp} \rightarrow \mathrm{et}$

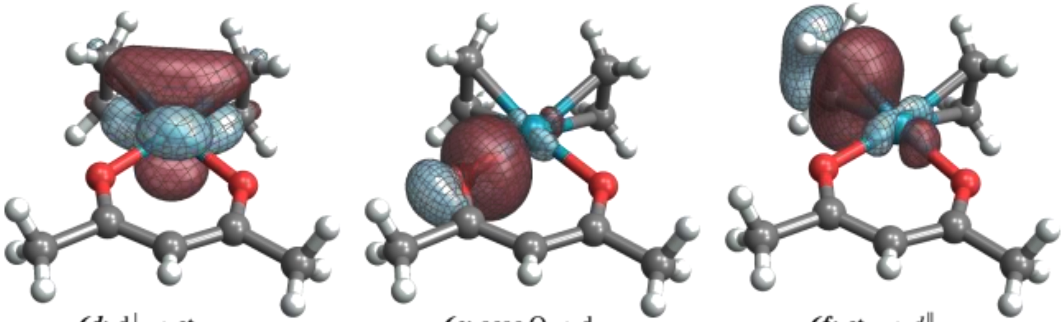

*6d*: $\mathrm{d}_{\pi}^{\perp} \rightarrow \mathrm{et}$ *6e*: acac O → d *6f*: $\mathrm{et}_{\pi} \rightarrow d^{\parallel}$

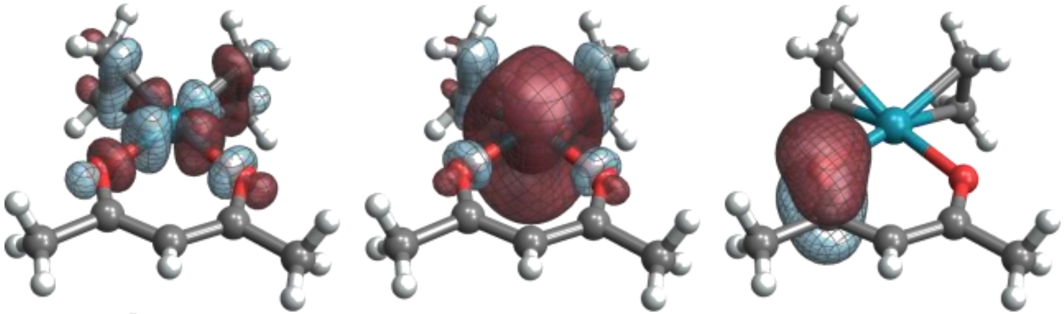

*6g*: $\mathrm{d}_{\sigma}^{\parallel}*$ *6h*: 5s-like $\sigma*$ *6i*: acac CO $\pi$

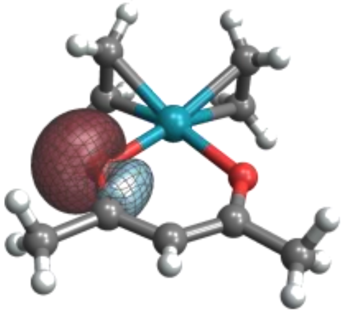

*6j*: acac O p

**Figure S13.** Isosurfaces for primary NLMOs contributing to the Rh isotropic shielding in Rh(et)$_2$(acac).

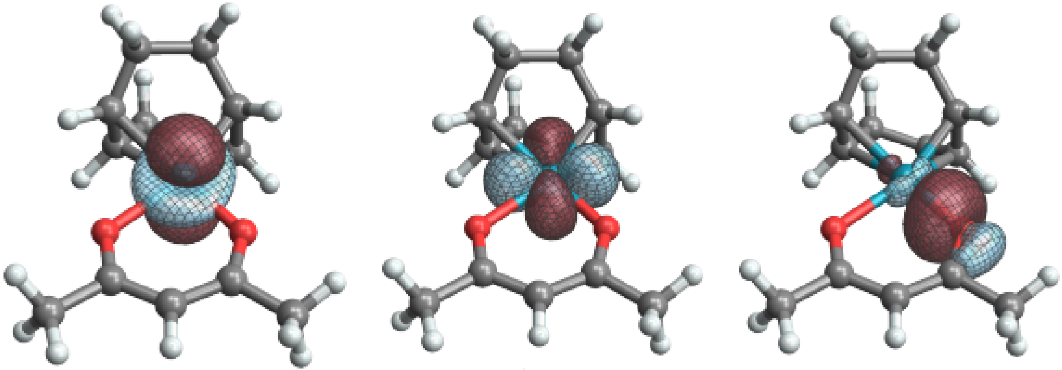

***7a***: $\mathrm{d}_{z^2}$ ***7b***: $\mathrm{d}_{xy}$ ***7c***: acac O → d

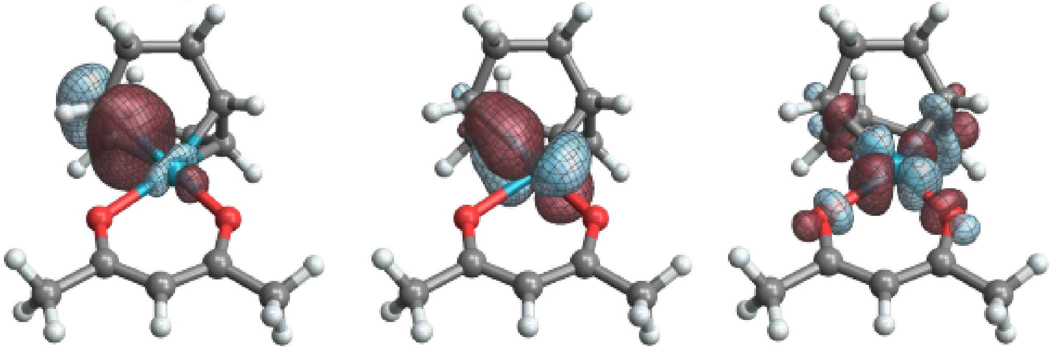

***7d***: $\mathrm{cod}_{\pi} \rightarrow d^{\parallel}$ ***7e***: $\mathrm{d}_{\delta}^{\perp} \rightarrow \mathrm{cod}$ ***7f***: $\mathrm{d}_{\sigma}^{\parallel}*$

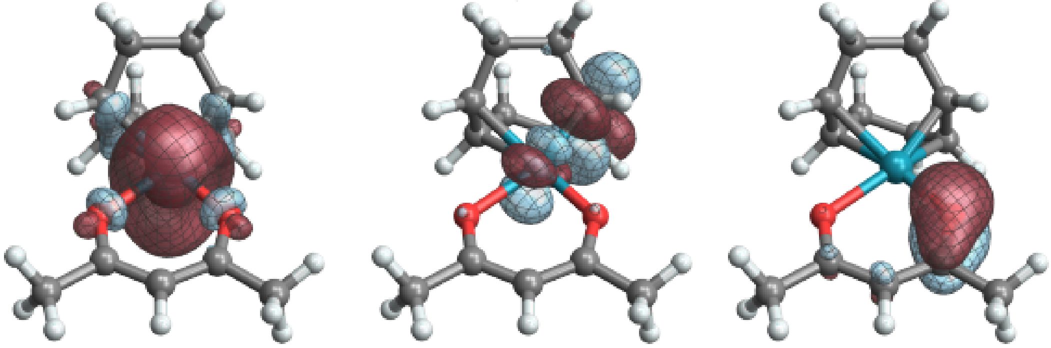

***7g***: 5s-like $\sigma*$ ***7h***: $\mathrm{d}_{\pi}^{\perp}*$ ***1i***: acac CO $\pi$

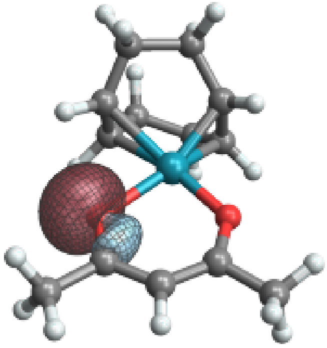

***7j***: acac O p

**Figure S14.** Isosurfaces for primary NLMOs contributing to the Rh isotropic shielding in Rh(cod)(acac).

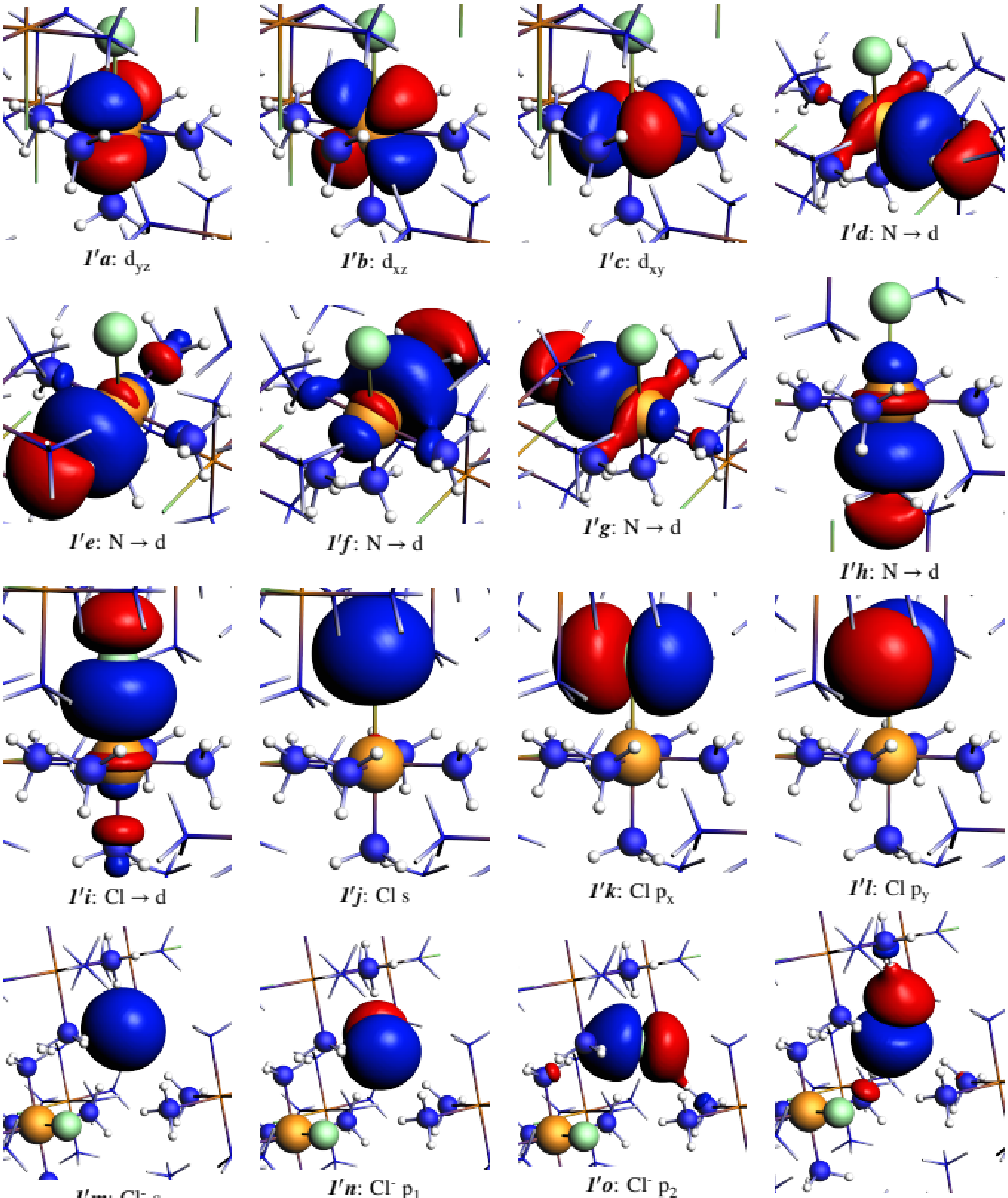

***1′a***: $d_{yz}$ ***1′b***: $d_{xz}$ ***1′c***: $d_{xy}$ ***1′d***: N → d

***1′e***: N → d ***1′f***: N → d ***1′g***: N → d ***1′h***: N → d

***1′i***: Cl → d ***1′j***: Cl s ***1′k***: Cl $p_x$ ***1′l***: Cl $p_y$

***1′m***: $Cl^-$ s ***1′n***: $Cl^-$ $p_1$ ***1′o***: $Cl^-$ $p_2$ ***1′p***: $Cl^-$ $p_3$

**Figure S15.** Isosurfaces for primary NLMOs contributing to the Rh isotropic shielding in the cluster model for the $[Rh(NH_3)_5Cl]Cl_2$ complex in the crystal.

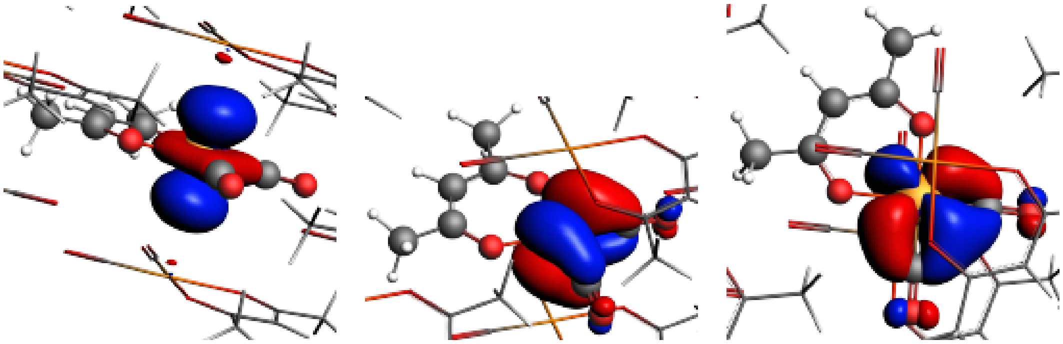

***3′a***: $\mathrm{d}_{z^2} \rightarrow \mathrm{CO}$ ***3′b***: $\mathrm{d}_{\pi} \rightarrow \mathrm{CO}$ ***3′c***: $\mathrm{d}_{\pi}^{\parallel} \rightarrow \mathrm{CO}$

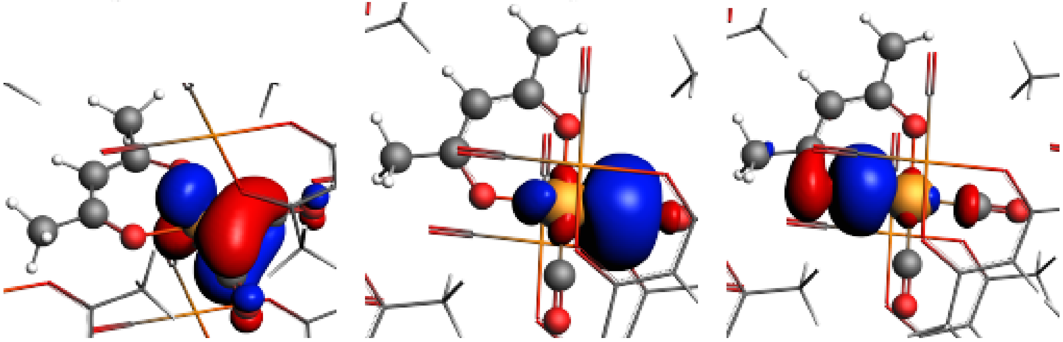

***3′d***: $\mathrm{d}_{\pi}^{\perp} \rightarrow \mathrm{CO}$ ***3′e***: $\mathrm{CO} \rightarrow \mathrm{d}^{\parallel}$ ***3′f***: $\mathrm{acac} \rightarrow \mathrm{d}^{\parallel}$

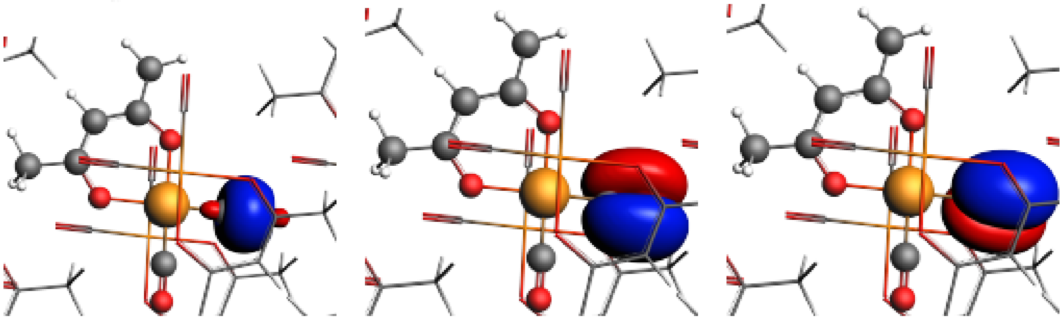

***3′g***: CO $\sigma$ ***3′h***: CO $\pi_1$ ***3′i***: CO $\pi_2$

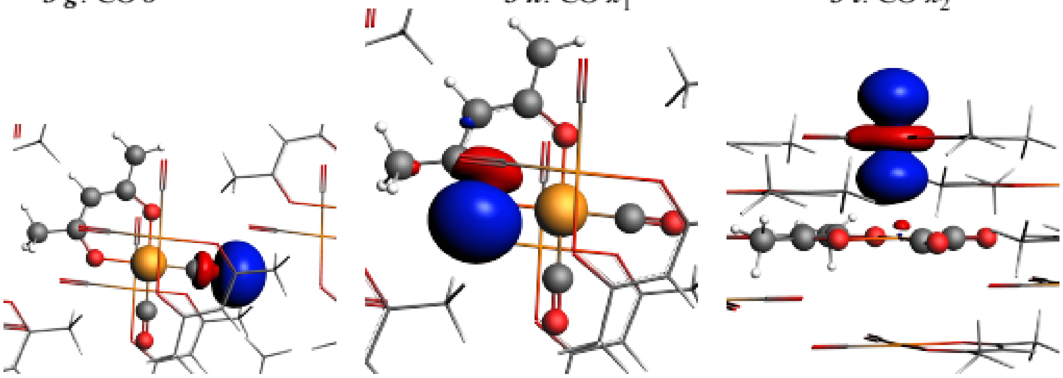

***3′j***: CO O LP ***3′k***: acac O LP ***3′l***: stacked Rh $\mathrm{d}_{z^2}$

**Figure S16.** Isosurfaces for primary NLMOs contributing to the Rh isotropic shielding in the cluster model of the Rh(CO)$_2$(acac) crystal.

**Table S1.** Some experimental parameters for the $^{1}H$-$^{103}Rh$ BRAIN-CP spectra shown in **Figures 1 - 2**.

| | | $[Rh(NH_3)_5Cl]Cl_2$ | $Rh(acac)_3$ | $Rh(CO)_2(acac)$ | $Rh(CO)_2Cp^*$ |
|---|---|---|---|---|---|
| Number of Transients | NS | 512 | 1024 | 1024 | 4096 |
| Recycle Delay (s) | D1 | 3 | 10 | 30 | 10 |
| Spectral Window (kHz) | SW | 300 | 100 | 500 | 300 |
| Dwell Time (μs) | DW | 1.667 | 5 | 1 | 1.667 |
| No. Meiboom-Gill loops | L22 | 20 | 19 | 130 | 70 |
| Spin Echo Length (μs) | D6 | 1200 | 1400 | 200 | 300 |
| Acquisition Time (ms) | AQ | 34.03 | 32.5 | 37.3 | 27.5 |
| Ring-down delay (μs) | DE | 10 | 10 | 10 | 10 |
| $^{1}H$ π/2 Pulse Length (μs) | P3 | 4.17 | 4.17 | 4.17 | 4.17 |
| $^{1}H$ π/2 Pulse rf (kHz) | P13 | 60 | 60 | 60 | 60 |
| $^{1}H$ CP Pulse rf (kHz) | SP0 | 25 | 25 | 25 | 25 |
| $^{1}H$ CW Decoupling Field (kHz) | P19 | 25 | 25 | 25 | 25 |
| WURST-A Length (μs) | P4 | 10 | 15 | 12 | 16 |
| WURST-A Sweep width (kHz) | Spnam4 | 50 | 50 | 150 | 150 |
| WURST-A rf (kHz) | SP4 | 25 | 25 | 25 | 25 |
| WURST-B Length (μs) | P5 | 25 | 25 | 25 | 25 |
| WURST-B Sweep width (kHz) | Spnam5 | 50 | 50 | 150 | 150 |
| WURST-B rf (kHz) | SP5 | 21 | 14.8 | 20 | 20 |

**Table S2.** More experimental parameters for the $^{1}$H-$^{103}$Rh BRAIN-CP spectra shown in **Figure 2**.

| | $[Rh(nbd)Cl]_2$ | $Rh(et)_2(acac)$ | Rh(cod)(acac) |
|---|---|---|---|
| Number of Transients | 1792 | 2048 | 1024 |
| Recycle Delay (s) | 30 | 30 | 20 |
| Spectral Window (kHz) | 625 | 1000 | 625 |
| Dwell Time (μs) | 0.8 | 0.5 | 1.6 |
| No. Meiboom-Gill loops | 100 | 90 | 50 |
| Spin Echo Length (μs) | 200 | 200 | 200 |
| Acquisition Time (ms) | 31.6 | 31.8 | 20.48 |
| Ring-down delay (μs) | 10 | 10 | 50 |
| $^{1}$H $\pi/2$ Pulse Length (μs) | 4.17 | 4.17 | 4.25 |
| $^{1}$H $\pi/2$ Pulse rf (kHz) | 60 | 60 | 58.82 |
| $^{1}$H CP Pulse rf (kHz) | 25 | 25 | ramp 22.9 to 18.5 |
| $^{1}$H CW Decoupling Field (kHz) | 25 | 25 | 20 |
| WURST-A Length (μs) | 16 | 15 | 30 |
| WURST-A Sweep width (kHz) | 400 | 400 | 400 |
| WURST-A rf (kHz) | 27 | 25 | 20.8 |
| WURST-B Length (μs) | 50 | 50 | 100 |
| WURST-B Sweep width (kHz) | 400 | 400 | 400 |
| WURST-B rf (kHz) | 24 | 21 | 16.4 |

**Table S3.** Experimental parameters for the $^{1}$H-$^{103}$Rh BRAIN-CP spectra shown in **Figures 3** and **S4**.

| | $Rh(acac)_3$ | $Rh(acac)_3$ | $Rh(CO)_2(acac)$ | $[Rh(nbd)Cl]_2$ |
|---|---|---|---|---|
| Field (T) | 21.1 | 35.2 | 35.2 | 35.2 |
| Number of Transients | 128 | 128 or 640 [a] | 832 | 1232 |
| Recycle Delay (s) | 10 | 10 | 30 | 30 |
| Spectral Window (kHz) | 500 | 147 | 500 | 1500 |
| Dwell Time (μs) | 1.00 | 3.40 | 1.00 | 0.333 |
| No. Meiboom-Gill loops | 50 | 40 | 90 | 80 |
| Spin Echo Length (μs) | 500 | 700 | 200 | 200 |
| Acquisition Time (ms) | 35.7 | 31.6 | 27.0 | 25.7 |
| Ring-down delay (μs) | 50 | 50 | 10.0 | 10 |
| $^{1}$H π/2 Pulse Length (μs) | 4.17 | 6.00 | 6.00 | 6.00 |
| $^{1}$H π/2 Pulse rf (kHz) | 60 | 41.67 | 41.67 | 41.67 |
| $^{1}$H CP Pulse rf (kHz) | 25 | 25 | 25 | 25 |
| $^{1}$H CW Decoupling Field (kHz) | 25 | 25 | 25 | 25 |
| WURST-A Length (μs) | 15 | 15 | 12 | 15 |
| WURST-A Sweep width (kHz) | 50 | 100 | 300 | 600 |
| WURST-A rf (kHz) | 25 | 25 | 25 | 25 |
| WURST-B Length (μs) | 25 | 25 | 50 | 75 |
| WURST-B Sweep width (kHz) | 50 | 100 | 300 | 600 |
| WURST-B rf (kHz) | 14.8 | 15.9 | 20.2 | 23.4 |

[a] The spectrum in Figure 3 was acquired with 128 scans, whereas the spectrum in Figure S4 was acquired with 640 scans.

**Table S4.** Experimental parameters for the $^{1}$H-$^{103}$Rh BRAIN-CP spectra shown in **Figures 4** and **S5**.

| | **Rh(cod)(acac)** | | **[RhCl(nbd)]$_2$** | | **Rh(et)$_2$(acac)** | |
|---|---|---|---|---|---|---|
| | Upper panel | Lower panel | Upper panel | Lower panel | Upper panel | Lower panel |
| Number of Transients | 2048 | 1024 | 2048 | 1792 | 1024 | 2048 |
| Recycle Delay (s) | 10 | 20 | 10 | 30 | 20 | 30 |
| Spectral Window (kHz) | 625 | 1000 | 625 | 625 | 625 | 1000 |
| Dwell Time (μs) | 1.6 | 0.5 | 1.6 | 0.8 | 1.6 | 0.5 |
| No. Meiboom-Gill loops | 50 | 90 | 50 | 100 | 50 | 90 |
| Spin Echo Length (μs) | 200 | 200 | 200 | 200 | 200 | 200 |
| Acquisition Time (ms) | 20.48 | 31.8 | 20.48 | 31.6 | 20.48 | 31.8 |
| Ring-down delay (μs) | 50 | 10 | 50 | 10 | 50 | 10 |
| $^{1}$H π/2 Pulse Length (μs) | 4.25 | 4.17 | 4.25 | 4.17 | 4.25 | 4.17 |
| $^{1}$H π/2 Pulse rf (kHz) | 58.82 | 60 | 58.82 | 60 | 58.82 | 60 |
| $^{1}$H CP Pulse rf (kHz) | ramp 23.5 to 18.6 | 25 | ramp 23.2 to 18.4 | 25 | ramp 22.9 to 18.5 | 25 |
| $^{1}$H CW Decoupling Field (kHz) | 20 | 25 | 20 | 25 | 20 | 25 |
| WURST-A Length (μs) | 30 | 15 | 30 | 16 | 30 | 15 |
| WURST-A Sweep width (kHz) | 400 | 400 | 400 | 400 | 400 | 400 |
| WURST-A rf (kHz) | 20.83 | 25 | 20.83 | 27 | 20.83 | 25 |
| WURST-B Length (μs) | 100 | 50 | 100 | 50 | 100 | 50 |
| WURST-B Sweep width (kHz) | 400 | 400 | 400 | 400 | 400 | 400 |
| WURST-B rf (kHz) | 16.4 | 21 | 17.05 | 24 | 16.4 | 21 |
| $^{1}$H flip-back pulse | yes | no | yes | no | yes | no |

**Table S5.** Crystallographic information and CSD/ICSD codes for all materials.

| Material | CSD Code | ICSD Code | Space Group |
|---|---|---|---|
| $[Rh(NH_3)_5Cl]Cl_2$ | – | 10199 | *Pnma* |
| $Rh(acac)_3$ | ACACRH10 | – | $P2_1/c$ |
| $Rh(CO)_2(acac)$ | ACABRH02 | – | $P\bar{1}$ |
| $Rh(CO)_2Cp^*$ | COXGUR | – | $P2_1/n$ |
| $[Rh(nbd)Cl]_2$ | ZOWVUC | – | $P2_1/c$ |
| Rh(cod)(acac) | COCAR | – | *Cc* |
| $Rh(et)_2(acac)$ | ACDERH01 | – | *Pnma* |

**Table S6.** Convergence of GIPAW calculations of $^{103}$Rh magnetic shielding tensors with respect to plane-wave cutoff energy and *k*-point spacing in $Rh(CO)_2(acac)$. [a]

| Cutoff energy (eV) | *k*-point spacing (Å$^{-1}$) | $\sigma_{11}$ (ppm) | $\sigma_{22}$ (ppm) | $\sigma_{33}$ (ppm) | Energy (eV × $10^{-4}$) |
|---|---|---|---|---|---|
| 600 | 0.08 | –1682 | –971 | 122 | –1.201085 |
| 600 | 0.07 | –1941 | –988 | 83 | –1.201088 |
| 600 | 0.06 | –1939 | –1222 | –152 | –1.201080 |
| 600 | 0.05 | –1939 | –1222 | –150 | –1.201080 |
| 500 | 0.05 | –1909 | –1229 | –170 | –1.200814 |
| 600 | 0.05 | –1939 | –1222 | –150 | –1.201080 |
| 700 | 0.05 | –1945 | –1214 | –148 | –1.201117 |
| 800 | 0.05 | –1941 | –1212 | –146 | –1.201121 |

[a] In these calculations, atomic coordinates were first optimized, followed by calculation of the $^{103}$Rh magnetic shielding tensor at the same level.

**Table S7.** Calculated $^{103}$Rh magnetic shielding tensors for isolated molecules using balanced and locally dense basis sets. [a,b]

| Material | Basis Set | $\sigma_{11}$ (ppm) | $\sigma_{22}$ (ppm) | $\sigma_{33}$ (ppm) | $d_v$ [c] (ppm) |
|---|---|---|---|---|---|
| $[Rh(NH_3)_5Cl]Cl_2$ | Balanced | –5069 | –4773 | –4762 | - |
| | Locally Dense | –5061 | –4755 | –4745 | 15 |
| $Rh(acac)_3$ | Balanced | –9598 | –9068 | –9024 | - |
| | Locally Dense | –9478 | –8955 | –8919 | 113 |
| $Rh(CO)_2(acac)$ | Balanced | –2342 | –403 | 984 | - |
| | Locally Dense | –2374 | –388 | 981 | 14 |
| $Rh(CO)_2Cp^*$ | Balanced | –167 | 871 | 1884 | - |
| | Locally Dense | –166 | 887 | 1852 | 14 |
| $[Rh(nbd)Cl]_2$ | Balanced | –6936 | 351 | 1224 | - |
| | Locally Dense | –6927 | 381 | 1239 | 19 |
| Rh(cod)(acac) | Balanced | –6296 | –291 | 1187 | - |
| | Locally Dense | –6293 | –226 | 1200 | 32 |
| $Rh(et)_2(acac)$ | Balanced | –6154 | 202 | 1510 | - |
| | Locally Dense | –6161 | 265 | 1524 | 30 |

[a] All calculations of $^{103}$Rh magnetic shielding tensors were performed at the PBE0/SO level.

[b] Balanced indicates that TZ2P was used for the entire molecule, whereas locally dense indicates that TZ2P was used for the rhodium atom and all directly bonded atoms, and DZ was used for all remaining atoms within the molecule.

[c] The chemical shift distance between the $^{103}$Rh magnetic shielding tensors (balanced *vs*. locally-dense basis sets).

**Table S8.** Summary of calculated $^{103}$Rh magnetic shielding tensors.

| Material | Method | Structure | $\sigma_{11}$ (ppm) | $\sigma_{22}$ (ppm) | $\sigma_{33}$ (ppm) |
|---|---|---|---|---|---|
| $[Rh(NH_3)_5Cl]Cl_2$ | GIPAW | Periodic | –4871 | –4871 | –4114 |
| | PBE/SR | Cluster | –4919 | –4900 | –4388 |
| | PBE/SO | Cluster | –6201 | –3496 | –2993 |
| | PBE0/SO | Cluster | –5839 | –5755 | –4961 |
| | PBE0/SO | Molecule | –5061 | –4755 | –4745 |
| $Rh(acac)_3$ | GIPAW | Periodic | –8114 | –7693 | –7595 |
| | PBE/SR | Cluster | –8039 | –7649 | –7500 |
| | PBE/SO | Cluster | –7444 | –7044 | –6901 |
| | PBE0/SO | Cluster | –9384 | –8880 | –8810 |
| | PBE0/SO | Molecule | –9478 | –8955 | –8919 |
| $Rh(CO)_2(acac)$ | GIPAW | Periodic | –1948 | –1220 | –164 |
| | PBE/SR | Cluster | –2131 | –1618 | –425 |
| | PBE/SO | Cluster | –1705 | –1281 | –12 |
| | PBE0/SO | Cluster | –2423 | –1178 | 267 |
| | PBE0/SO | Molecule | –2374 | –388 | 981 |
| $Rh(CO)_2Cp^*$ | GIPAW | Periodic | –84 | 685 | 1554 |
| | PBE/SR | Cluster | –171 | 556 | 1393 |
| | PBE/SO | Cluster | 249 | 945 | 1795 |
| | PBE0/SO | Cluster | –111 | 865 | 1829 |
| | PBE0/SO | Molecule | –166 | 887 | 1852 |
| $[Rh(nbd)Cl]_2$ | GIPAW | Periodic | –8256 | 972 | 1875 |
| | PBE/SR | Cluster | –6030 | 40 | 580 |
| | PBE/SO | Cluster | –5527 | 407 | 999 |
| | PBE0/SO | Cluster | –6866 | 412 | 1287 |
| | PBE0/SO | Molecule | –6927 | 381 | 1239 |
| Rh(cod)(acac) | GIPAW | Periodic | –5165 | –161 | 450 |
| | PBE/SR | Cluster | –5170 | –525 | 476 |
| | PBE/SO | Cluster | –4705 | –113 | 861 |
| | PBE0/SO | Cluster | –6301 | –158 | 1204 |
| | PBE0/SO | Molecule | –6293 | –226 | 1200 |
| $Rh(et)_2(acac)$ | GIPAW | Periodic | –6304 | 346 | 1879 |
| | PBE/SR | Cluster | –5160 | –233 | 741 |
| | PBE/SO | Cluster | –4688 | 140 | 1147 |
| | PBE0/SO | Cluster | –6248 | 183 | 1463 |
| | PBE0/SO | Molecule | –6161 | 265 | 1524 |

**Table S9.** Summary of NLMO contributions to $^{103}$Rh isotropic shielding for isolated rhodium complexes (absent crystal embedding).

| | $[Rh(NH_3)_5Cl]Cl_2$ (1) | $Rh(acac)_3$ (2) | $Rh(CO)_2(acac)$ (3) | $Rh(CO)_2Cp^*$ (4) | $[Rh(nbd)Cl]_2$ (5) | $Rh(et)_2(acac)$ (6) | $Rh(cod)(acac)$ (7) |
|---|---|---|---|---|---|---|---|
| Rh 4d | -2857 [***1a***: $d_{yz}$]<br>-2846 [***1b***: $d_{xz}$]<br>-2970 [***1c***: $d_{xy}$] | -4245 [***2a***]<br>-4253 [***2b***]<br>-3986 [***2c***] | -943 [***3a***]<br>-791 [***3b***]<br>-2134 [***3c***+***3d***][a] | -1007 [***4a***]<br>-581 [***4b***]<br>-947 [***4c***]<br>-463 [***4d***] | -1001 [***5a***]<br>-3451 [***5b***]<br>-523 [***5c***] | -862 [$d_{z2}$]<br>-3495 [$d_{xy}$]<br>-580 [***6c***]<br>-366 [***6d***] | -852 [$d_{z2}$]<br>-3339 [$d_{xy}$] |
| ∑above 4d | -8673 | -12483 | -3868 | -2998 | -4975 | -5303 | -4191 |
| Rh core | 4238 | 4384 | 4226 | 4172 | 4355 | 4383 | 4352 |
| Rh–X | -241 [***1d***(5)][d]<br>-25 [***1e***] | -510 [***2d***(6)][d]<br>-60 [***2e***(3)][d] | -464 [***3e***(2)][d]<br>-316 [***3f***(2)][d] | 36 [***4e***(2)] [d]<br>-422 [***4f***(2)][d] | -436 [***5d***(2)+***5e***][a,d]<br>-459 [***5f***(4)][a,d] | -338 [***6e***(2)][d]<br>-140 [***6f***(2)][d]<br>-18 [***6g***]<br>4 [***6h***] | -300 [***7c***(2)][d]<br>-1529 [***7d***(2)+***7e***(2)][a,d]<br>-16 [***7f***]<br>2 [***7g***]<br>-3 [***7h***] |
| Other Bonding | -30 [***1f***(15)][d] | -140 [***2f***(6)][d]<br>-88 [all acac σ] | -46 [***3g***(2)][d]<br>-25 [***3h***(2)+***3i***(2)][d] | -77 [***4g***(2)+***4h***(2)+***4i***(2)][d]<br>176 [***4j***+***4k***] | -173 [***5g***(2)+***5h***][a,d] | 44 [all et σ]<br>-29 [all acac σ]<br>17 [***6i***(2)][d] | 4 [all cod σ]<br>-28 [all acac σ]<br>17 [***7i***(2)][d] |
| Other LP | -8 [Cl s] [***1j***]<br>-5 [Cl $p_x$+$p_y$][***1k***+***1l***] | -162 [***2g***(6)][d] | -21 [***3j***(2)][d]<br>-24 [***3k***(2)][d] | -19 [2 CO O] | -20 [***5i***(2)][d]<br>7 [***5j***(2)][d]<br>-12 [***5k***+***5l***] | -33 [***6j***(2)][d] | -35 [***7j***(2)][d] |
| Other occ. | 1 | -2 | -3 | 21 | 12 | 7 | 9 |
| Unocc. [b] | -77 | -49 | -48 | -26 | -71 | -51 | -47 |
| Total [c] | -4819 | -9112 | -588 | 864 | -1773 | -1456 | -1765 |

[a] Where indicated, the calculation produced one or more pairs of NLMOs with mixed in-plane vs. out-of-place local π symmetry. For the purpose of visualization, linear combinations of these NLMOs with clean symmetries were generated. The combined shielding contributions from these orbitals are the same for the original NLMOs and the symmetry-adapted linear combinations. In some cases, the contributions are grouped with other NLMOs of matching symmetry.

[b] By construction, the scalar relativistic NLMOs have occupations of either 2 or 0. Contributions shown from unoccupied orbitals come about because of the SO electronic calculation modifying the ground-state density relative to that of the parent scalar relativistic calculation.

[c] Rounded from sum of contributions at full numerical precision.

[d] Numbers in parentheses indicate combined contributions from many equivalent NLMOs.

**Table S10.** Summary of NLMO contributions to $^{103}$Rh shielding span ($\Omega = \sigma_{33} - \sigma_{11}$) for isolated rhodium complexes (absent crystal embedding).

| | [Rh(NH$_3$)$_5$Cl]$^{2+}$ **(1)** | Rh(acac)$_3$ **(2)** | Rh(CO)$_2$(acac) **(3)** | Rh(CO)$_2$Cp$^*$ **(4)** | [Rh(nbd)Cl]$_2$ **(5)** | Rh(et)$_2$(acac) **(6)** | Rh(cod)(acac) **(7)** |
|---|---|---|---|---|---|---|---|
| Rh 4d | 350 [***1a***: d$_{yz}$]<br>-8586 [***1b***: d$_{xz}$]<br>8544 [***1c***: d$_{xy}$] | 3352 [***2a***]<br>3394 [***2b***]<br>-6111 [***2c***] | -868 [***3a***]<br>-62 [***3b***]<br>3627 [***3c***+***3d***]$^{a}$ | -393 [***4a***]<br>-42 [***4b***]<br>2618 [***4c***]<br>-840 [***4d***] | -686 [***5a***]<br>8567 [***5b***]<br>249 [***5c***] | -823 [d$_{z2}$] [***6a***]<br>8827 [d$_{xy}$] [***6b***]<br>227 [***6c***]<br>-645 [***6d***] | -1055 [d$_{z2}$] [***7a***]<br>8269 [d$_{xy}$] [***7b***] |
| ∑above 4d | 309 | 635 | 2697 | 1343 | 8130 | 7585 | 7213 |
| Rh core | 100 | -32 | 406 | 90 | 150 | 163 | 190 |
| Rh–X | -11 [***1d***(5)]$^{d}$<br>-55 [***1e***] | 74 [***2d***(6)]$^{d}$<br>4 [***2e***(3)]$^{d}$ | 289 [***3e***(2)]$^{d}$<br>-213 [***3f***(2)]$^{d}$ | 305 [***4e***(2)]$^{d}$<br>-85 [***4f***(2)]$^{d}$ | -307 [***5d***(2)+***5e***]$^{a,d}$<br>-262 [***5f***(4)]$^{a,d}$ | -407 [***6e***(2)]$^{d}$<br>146 [***6f***]<br>37 [***6g***]<br>3 [***6h***] | -281 [***7c***(2)]$^{d}$<br>144 [***7d***(2)+***7e***(2)]$^{a,d}$<br>35 [***7f***]<br>5 [***7g***]<br>6 [***7h***] |
| Other Bonding | -35 [***1f***(15)]$^{d}$ | 82 [***2f***(6)]$^{d}$<br>9 [all acac σ] | 49 [***3g***(2)]$^{d}$<br>41 [***3h***(2)+***3i***(2)]$^{d}$ | 76 [***4g***(2)+***4h***(2)+***4i***(2)]$^{d}$<br>306 [***4j***+***4k***] | 250 [***5g***(2)+***5h***]$^{a,d}$ | 122 [all et σ]<br>-15 [all acac σ]<br>21 [***6i***(2)]$^{d}$ | 136 [all cod σ]<br>-11 [all acac σ]<br>14 [***7i***(2)]$^{d}$ |
| Other LP | -12 [Cl s] [***1j***]<br>-45 [Cl p$_x$+p$_y$] [***1k***+***1l***] | -67 [***2g***(6)]$^{d}$ | 27 [***3j***(2)]$^{d}$<br>28 [***3k***(2)]$^{d}$ | 25 [2 CO O] | -25 [***5i***(2)]$^{d}$<br>16 [***5j***(2)]$^{d}$<br>33 [***5k***+***5l***] | 26 [***6j***(2)]$^{d}$ | 25 [***7j***(2)]$^{d}$ |
| Other occ. | -1 | -3 | -29 | -70 | 114 | -35 | -28 |
| Unocc. $^{b}$ | 1 | 6 | 30 | 25 | 82 | 30 | 32 |
| Total $^{c}$ | 319 | 559 | 3326 | 2015 | 8181 | 7676 | 7480 |

[a] Where indicated, the calculation produced one or more pairs of NLMOs with mixed in-plane vs. out-of-place local π symmetry. For the purpose of visualization, linear combinations of these NLMOs with clean symmetries were generated. The combined shielding contributions from these orbitals are the same for the original NLMOs and the symmetry-adapted linear combinations. In some cases, the contributions are grouped with other NLMOs of matching symmetry.

[b] By construction, the scalar relativistic NLMOs have occupations of either 2 or 0. Contributions shown from unoccupied orbitals come about because of the SO electronic calculation modifying the ground-state density relative to that of the parent scalar relativistic calculation.

[c] Rounded from sum of contributions at full numerical precision.

[d] Numbers in parentheses indicate combined contributions from many equivalent NLMOs.

**Table S11.** Summary of NLMO contributions to $^{103}$Rh isotropic shielding for rhodium complexes in a cluster-model crystal embedding.

| | $[Rh(NH_3)_5Cl]Cl_2$ (**1′**) | $Rh(CO)_2(acac)$ (**3′**) |
|---|---|---|
| Rh 4d | -3149 [***1′a***: $d_{yz}$]<br>-3182 [***1′b***: $d_{xz}$]<br>-2915 [***1′c***: $d_{xy}$] | -1183 [***3′a***]<br>-844 [***3′b***]<br>-1560 [***3′c***]<br>-650 [***3′d***] |
| ∑ 4d | -9246 | -4237 |
| Rh core | 4194 | 4224 |
| Rh–X | -223 [***1′d–h***]<br>-25 [***1′i***] | -462 [***3′e***(2)][c]<br>-270 [***3′f***(2)][c] |
| Other Bonding | -62 [N–H(15)] [c] | -44 [***3′g***(2)][c]<br>-27 [***3′h***(2)+***3′i***(2)][c] |
| Other LP | -8 [Cl s] [***1′j***]<br>-45 [***1′k***(8)+***1′l***(8)][c]<br>22 [***1′m–p*** (8)][c] | -21 [***3′j***(2)][c]<br>-31 [***3′k***(2)][c]<br>-88 [***3′l***(2)] |
| Other occc. | -7 | -99 |
| Unocc. [a] | -82 | -49 |
| Total [b] | -5481 | -1104 |

[a] By construction, the scalar relativistic NLMOs have occupations of either 2 or 0. Contributions shown from unoccupied orbitals come about because of the SO electronic calculation modifying the ground-state density relative to that of the parent scalar relativistic calculation.

[b] Rounded from sum of contributions at full numerical precision.

[c] Numbers in parentheses indicate combined contributions from that many equivalent NLMOs.

**Supplement 1: Chemical Shift Distance.** The relationship between calculated principal components of the $^{103}$Rh magnetic shielding tensors ($\sigma_{ii}^{v,\mathrm{calc}}$) and experimental principal components of $^{103}$Rh chemical shift tensors ($\delta_{ii}^{v,\mathrm{exp}}$) is described by the following expression:

$$\sigma_{ii}^{v,\mathrm{exp}} = A\delta_{ii}^{v,\mathrm{calc}} + B. \qquad \textbf{(1)}$$

where the index $v$ denotes the rhodium site ($v = 1, 2, \ldots, N$), the index $i$ denotes the principal component of the shielding tensor ($i = 1, 2, 3$), $A$ represents the slope of the correlation line, and $B$ represents the interpolated shielding of the reference state. Calculated chemical shifts ($\delta_{ii}^{v,\mathrm{calc}}$) are derived from the following expression:

$$\delta_{ii}^{v,\mathrm{calc}} = (B - \sigma_{ii}^{v,\mathrm{calc}})/A. \qquad \textbf{(2)}$$

The *chemical shift distance* for atom $v$, $d_v$, provides a comparison between a calculated and experimental chemical shift tensor with a single scalar value in ppm. Given two sets of principal components of chemical shift tensors, $d_v$ is defined by the following expression:

$$\begin{aligned} d_v = \bigg(\frac{1}{15}\Big[&3\big(\delta_{11}^{v,\mathrm{calc}} - \delta_{11}^{v,\mathrm{exp}}\big)^2 + 3\big(\delta_{22}^{v,\mathrm{calc}} - \delta_{22}^{v,\mathrm{exp}}\big)^2 \\ &+ 3\big(\delta_{33}^{v,\mathrm{calc}} - \delta_{33}^{v,\mathrm{exp}}\big)^2 \\ &+ 2\big(\delta_{11}^{v,\mathrm{calc}} - \delta_{11}^{v,\mathrm{exp}}\big)\big(\delta_{22}^{v,\mathrm{calc}} - \delta_{22}^{v,\mathrm{exp}}\big) \\ &+ 2\big(\delta_{11}^{v,\mathrm{calc}} - \delta_{11}^{v,\mathrm{exp}}\big)\big(\delta_{33}^{v,\mathrm{calc}} - \delta_{33}^{v,\mathrm{exp}}\big) \\ &+ 2\big(\delta_{22}^{v,\mathrm{calc}} - \delta_{22}^{v,\mathrm{exp}}\big)\big(\delta_{33}^{v,\mathrm{calc}} - \delta_{33}^{\mathrm{exp}}\big)\Big]\bigg)^{1/2}. \end{aligned} \qquad \textbf{(3)}$$

A root-mean-square chemical shift distance for an ensemble of $N$ chemical shift tensors ($\Delta_{\mathrm{RMS}}$) is determined by the following expression:

$$\Delta_{\mathrm{RMS}} = \left(\frac{1}{N}\sum_{v=1}^{N} d_v^2\right)^{1/2}. \qquad \textbf{(4)}$$